

HAWK-I imaging of the X-ray luminous galaxy cluster XMMU J2235.3-2557^{*}

The red sequence at $z = 1.39$

C. Lidman¹, P. Rosati², M. Tanaka², V. Strazzullo³, R. Demarco⁴, C. Mullis⁵, N. Ageorges⁶, M. Kissler-Patig², M. G. Petr-Gotzens², and F. Selman¹

¹ European Southern Observatory, Alonso de Cordova 3107, Casilla 19001, Santiago, Chile

² European Southern Observatory, Karl-schwarzschild-Strasse 2, D-85748 Garching, Germany

³ National Radio Astronomy Observatory, P.O. Box O, Socorro, NM, 87801, USA

⁴ Department of Physics and Astronomy, John Hopkins University, Baltimore, USA

⁵ Wachovia Corporation, NC6740, 100 N. Main Street, Winston-Salem, NC 27101

⁶ MPI für extraterrestrische Physik, Giessenbachstrasse, D-85748 Garching, Germany

Received July 9, 2008; accepted July 31, 2008

ABSTRACT

We use HAWK-I, the recently-commissioned near-IR imager on Yepun (VLT-UT4), to obtain wide-field, high-resolution images of the X-ray luminous galaxy cluster XMMU J2235.3-2557 in the J and Ks bands, and we use these images to build a colour-magnitude diagram of cluster galaxies. Galaxies in the core of the cluster form a tight red sequence with a mean J – Ks colour of 1.9 (Vega system). The intrinsic scatter in the colour of galaxies that lie on the red sequence is similar to that measured for galaxies on the red sequence of the Coma cluster. The slope and location of the red sequence can be modelled by passively evolving the red sequence of the Coma cluster backwards in time. Using simple stellar population (SSP) models, we find that galaxies in the core of XMMU J2235.3-2557 are, even at $z = 1.39$, already 3 Gyr old, corresponding to a formation redshift of $z_f \sim 4$. Outside the core, the intrinsic scatter and the fraction of galaxies actively forming stars increase substantially. Using SSP models, we find that most of these galaxies will join the red sequence within 1.5 Gyr. The contrast between galaxies in the cluster core and galaxies in the cluster outskirts indicates that the red sequence of XMMU J2235.3-2557 is being built from the dense cluster core outwards.

Key words. Galaxies:clusters:general – Galaxies:clusters:individual XMMU J2235.3-2557 – Galaxies:evolution

1. Introduction

The most notable feature in the colour-magnitude (C-M) diagram of a rich galaxy cluster is the tight red sequence of passively-evolving galaxies. First observed in nearby galaxy clusters (e.g., de Vaucouleurs 1961; Visvanathan & Sandage 1977), it has also been observed in some of the most distant galaxy clusters currently known (e.g., van Dokkum et al. 2001; Blakeslee et al. 2003; Lidman et al. 2004; Holden et al. 2004; Mei et al. 2006).

The location and tightness of the red sequence are used to infer that the bulk of the stars in red sequence galaxies formed over a relatively short space of time at much higher redshifts (Bower et al. 1992; Stanford et al. 1998). In RDCS J1252-2927 at $z = 1.24$, for example, Blakeslee et al. (2003) find that most of the stars in the galaxies that lie on the red sequence formed 11.9 Gyr ago.

The red sequence is tilted in the sense that brighter galaxies are also redder. The tilt is understood as a relationship between mass and metallicity (Kodama 1999; Gallazzi et al. 2006). Brighter, more massive galaxies are more metal rich and are hence redder. The tilt is observed at all redshifts, and there is little evidence that it evolves by more than that expected from pas-

sive evolution of an old stellar population (Stanford et al. 1998; Blakeslee et al. 2003). However, there are hints that it flattens at the bright end for some $z > 1$ clusters (van Dokkum et al. 2001; Demarco et al. 2007) and for S0 galaxies in the cluster RDCS J0910+5422 at $z = 1.106$ (Mei et al. 2006).

When sufficiently precise measurements have been made, the sequence has a small, but non-zero, scatter in colour (Bower et al. 1992; Eisenhardt et al. 2007). For the most massive clusters, the scatter appears to be independent of redshift (Stanford et al. 1998; van Dokkum et al. 2001; Blakeslee et al. 2003; Mei et al. 2006; Homeier et al. 2006); however, in some less massive clusters (Holden et al. 2004), the scatter is larger and the red sequence is less regular. While it is generally accepted that the tilt in the colour-magnitude relation is primarily the result of a relationship between mass and metallicity, the reasons for the scatter are less clear. For early-type galaxies in the field, the scatter is caused by differences in age and metallicity, with variations in metallicity playing an increasingly important role as the mass of the galaxy increases (Gallazzi et al. 2006). Dust could also play a role.

Within the framework of hierarchical structure formation, one expects the morphology of the red sequence to evolve as one approaches the epoch of cluster formation. The major processes are thought to be: passive evolution of old stellar populations, conversion of galaxies that are in the “blue cloud” into red ones through the quenching of star formation, and dry mergers

^{*} Based on observations obtained at the European Southern Observatory using the ESO Very Large Telescope on Cerro Paranal through ESO program 060.A-9284(H).

(Bell et al. 2006; Faber et al. 2007). The time at which these processes initiate and the speed at which they run depend on environment, with the result that the red sequences of the most massive clusters form first (Tanaka et al. 2005; Romeo et al. 2008; Menci et al. 2008).

Recent observations of the most distant clusters have started to note changes in the morphology of the red sequence. A deficit of galaxies at the faint end of the red sequence has been noted in the large scale structure surrounding the high redshift cluster RDCS J1252-2927 at $z = 1.24$ (Tanaka et al. 2007). A similar deficit in the cluster itself was not seen, suggesting that the rate at which the red sequence develops depends on environment, as one expects in hierarchical models and as seen in some clusters at lower redshifts (Tanaka et al. 2005). The faint end deficit has been noted in clusters from the ESO distant cluster survey (De Lucia et al. 2004b, 2007); however, no such deficit was found in the cluster sample that was analysed by Andreon (2008), perhaps indicating that the clusters analysed by Andreon were, on average, richer than those in ESO distant cluster survey. A similar richness dependence was noted in clusters from the Red Cluster Survey (Gilbank et al. 2008).

In a recent study of several proto-clusters with redshifts ranging from $z = 2.2$ to $z = 3.1$, Kodama et al. (2007) found that the bright end of the red sequence becomes progressively less well defined as the redshift of the proto-cluster increases. In one of the most well-studied proto-clusters, PKS 1138-262 at $z = 2.16$, Zirm et al. (2008) found that the red sequence of PKS 1138-262 is considerably less well defined than the red sequence of rich clusters at lower redshifts.

Hence, between the redshift of most well studied clusters at $z \sim 1.3$ and the most well studied proto-clusters at $z \sim 2$, there is evidence for a dramatic change in the morphology of the red sequence. Massive X-ray luminous clusters beyond a redshift of 1.3 are rare, and currently, only 2 are known, XMMU J2235.3-2557 (Mullis et al. 2005) at $z = 1.39$ and XMMXCS J2215.9-1738 at $z = 1.45$ (Stanford et al. 2006).

In this paper, we present the near-IR colour-magnitude (C-M) diagram of XMMU J2235.3-2557, one of the most distant X-ray luminous clusters currently known. In section 2 of the paper, we describe the near-IR observations and the methods used to process the data. In section 3, we present the C-M diagram and derive the intrinsic scatter in the colour of galaxies that lie on the red sequence. In section 4, we discuss the results. Throughout this paper, we assume a flat, Λ -dominated universe with $\Omega_M = 0.27$ and $H_0 = 71 \text{ km s}^{-1} \text{ Mpc}^{-1}$. In this cosmology, $1''$ on the sky corresponds to 8.5 kpc at $z = 1.39$. Unless specified otherwise, all magnitudes are Vega magnitudes and are on the 2MASS system. In a forthcoming paper, we will present an analysis of multi-wavelength observations of XMMU J2235.3-2557, including spectroscopy from VLT/FORS2 and optical imaging from ACS/HST.

2. Observations and Photometry

2.1. Observations

XMMU J2235.3-2557 was observed with HAWK-I (Pirard et al. 2004; Casali et al. 2006, Kissler-Patig et al. in preparation) on Yepun (VLT-UT4) at the ESO Cerro Paranal Observatory. The observations were taken in service mode during the first two weeks of October 2007 as part of the first HAWK-I science verification run.

HAWK-I is a near-IR imager with a 7.5×7.5 field of view. The focal plane consists of a mosaic of 4 Hawaii-2RG detectors

and results in an average pixel scale of $0''.1065$ per pixel. The cluster was imaged in J and Ks.

In order to avoid the gaps between the detectors in the mosaic and to cover a wide area, the observations were not done with the cluster positioned in the centre of the mosaic. Instead, a series of four pointings with the cluster positioned in the four outer corners of the mosaic was used. The resulting union of images covers 13.5 by 13.5 of the sky without gaps.

Individual exposures lasted 10 seconds in both J and Ks, and 12 (6 for Ks) of these were averaged to form a single image. Between images, the telescope was moved by $10''$ to $30''$ in a semi-random manner, and 22 to 45 images were taken in this way in a single observing block. In the cluster centre, which was always imaged, the total exposure times for J and Ks were 176 and 179 minutes, respectively. Exposure times and detection limits are reported in Table 1.

Standards were selected from the LCO (Persson et al. 1998) and UKIRT (Hawarden et al. 2001) standard star lists. The UKIRT standards were used to monitor the transparency of the nights, which were stable to within 2% during the period the cluster was observed. The LCO standards were used to set the zero point.

2.2. Data Processing

The processing of the raw data was done in a standard manner and consisted of the following steps:

1. subtraction of dark frames to remove the zero-level offset
2. division by normalised twilight flats to normalise the pixel-to-pixel response
3. object masked sky subtraction using the XDIMSUM package in IRAF¹
4. normalisation of the detector gains using the instrumental magnitudes of the UKIRT and LCO standards.
5. astrometric calibration using SExtractor (version 2.5.0) and SCAMP (version 1.4.0)²
6. image combination using SWarp (version 2.16.4)²

The mean count level in the raw images varies from 2,000 ADU in 10 seconds for J to 10,000 ADU in 10 seconds for Ks. Since the 1% non-linearity threshold is 30,000 ADU, corrections for detector non-linearity were not applied.

The accuracy of the flat fielding over the HAWK-I field of view was tested by observing stars over a 5×5 or 9×9 grid. For sufficiently bright stars, the dispersion in the instrumental magnitude of any one star was never greater than 0.02 magnitudes.

The accuracy of the zero points were assessed by comparing the magnitudes of stars in the HAWK-I images with the magnitudes listed in the 2MASS point source catalogue (Skrutskie et al. 2006). For stars in the magnitude range $13.5 < J_{2MASS} < 15.5$ ($13 < K_{S2MASS} < 15$ for Ks) the difference $J_{HAWK-I} - J_{2MASS}$, averaged over 26 stars, was 0.025 magnitudes (for Ks, $K_{S,HAWK-I} - K_{S2MASS} = 0.010$ magnitudes, averaged over 30 stars). Stars brighter than 13.5 magnitudes in J and 13 magnitudes in Ks were saturated in the HAWK-I images.

The fully processed frames were co-added to produce two sets of images. In the first set, all frames with a given filter were co-added to produce a deep image of the centre of the cluster.

¹ IRAF is distributed by the National Optical Astronomy Observatories which are operated by the Association of Universities for Research in Astronomy, Inc., under the cooperative agreement with the National Science Foundation

² <http://terapix.iap.fr>

Table 1. Exposure times, image quality and detection limits of the reduced HAWK-I data.

Filter	Exposure time ^a (seconds)	Image quality ($''$)	Detection limit ^b (Vega magnitudes)
J	10560	0.47	24.9
Ks	10740	0.32	23.2

^a All quantities refer to the central part of the mosaic, where exposure times are greatest.

^b The detection limit is the 5 sigma point source detection limit within an aperture that has a diameter equal to twice the image quality.

In the second set, the frames corresponding to a single pointing were co-added together. With four pointings, this results in four images per filter. In both sets and for the purpose of maximising image quality, individual frames are weighted by the square of the inverse of the FWHM of stars in those frames. This results in five pairs of images, one for the centre of the cluster and four for the cluster outskirts. Each image pair is then processed (the image with the best image quality is smoothed with a Moffat function) so that the image quality within that pair match. The separation between the core of the cluster, which is common to all frames, and the cluster outskirts, which are not common to all frames, facilitates the task of computing colours from aperture magnitudes.

2.3. Object Detection and Photometry

The analysis is split into two regions: the central arc-minute of the cluster, which is common to all frames, and the region that is outside of this.

For the central arc minute of the mosaic, we used version 2.5.0 of SExtractor (Bertin & Arnouts 1996) in double image mode to detect objects in the unsmoothed Ks-band image and to measure aperture magnitudes in the smoothed and aligned images. The aperture diameter is set to 9 pixels ($0''.96$ or 8 kpc at the redshift of the cluster), which is about twice the FWHM of point sources in the J-band image. We use the SExtractor neural network classifier to separate stars from galaxies.

For regions outside the central arc minute we used SExtractor in single image mode to measure aperture magnitudes in the smoothed and aligned images. To simplify the analysis and to reduce errors caused by slight misalignments, the aperture is set to 12 pixels.

For both the central region and the region outside of it, colours are estimated from aperture magnitudes.

Total magnitudes are estimated differently. Given the crowded nature of the centre of the cluster, we use version 2.0.3c of GALFIT (Peng et al. 2002) on the unsmoothed Ks-band images to estimate total Ks magnitudes. In crowded regions, the MAG_AUTO estimate of SExtractor systematically overestimates the flux of galaxies that lie within the detection isophote of a brighter neighbour. For isolated galaxies, GALFIT and SExtractor MAG_AUTO magnitudes agree with a dispersion of 0.2 magnitudes.

The central wavelength of the HAWK-I J filter is slightly redder than the 2MASS J filter, so we expect a small colour term when transferring from HAWK-I colours to 2MASS colours. To estimate the colour term, we used the transmission

curves of the HAWK-I³ and 2MASS (Cohen et al. 2003) filters and a range of theoretical galaxy spectral energy distributions (Bruzual & Charlot 2003). We find

$$(J - Ks)_{2MASS} = 1.032 (J - Ks)_{HAWK-I} - 0.025 \quad (1)$$

Note that this transformation is strictly valid for the spectral energy distributions (SED) that were used to compute it. It is unlikely to be valid for other SEDs. In particular, late type stars, because of their broad spectral features, will require a different relation.

The Galactic extinction along the line of sight to XMMU J2235.3-2557 was estimated from the dust maps of Schlegel et al. (1998). The extinction is 0.019 and 0.008 magnitudes in J and Ks, respectively, and both colours and total magnitudes were corrected for it.

2.4. Photometric errors

In order to obtain a reliable estimate of the location of the red sequence and the scatter within it, it is important to quantify random and systematic errors.

In the fully processed images, the noise between pixels is correlated. This is caused by the interpolation that is used when aligning images, and by large scale features in the sky background (Labbé et al. 2003). The end result is that the dispersion in the flux integrated over a fixed aperture is underestimated if one simply scales the noise in a single pixel by the square root of the number of pixels in the aperture.

To overcome this difficulty, the error in the flux in an aperture of a certain size is estimated by randomly placing these apertures in regions that are free of detectable objects and by computing the dispersion in the integrated flux. The dispersion is then combined with the object flux to compute a magnitude error.

In addition to random errors caused by photon shot noise, there are systematic errors that can affect the location of the red sequence in the C-M diagram and the scatter within the sequence itself. We discuss likely sources of systematic error and assess their impact.

The correction that is applied for the difference between the HAWK-I and 2MASS filters (Eq. 1) is possibly one of the largest sources of systematic error. However, without observational data to validate the correction that is applied in Eq. 1, it is difficult to assess the accuracy of the correction and to assign a systematic error. So, we do not assign an error, but note that it might be significant if the filters are very different to those that are published, or if the spectra of high redshift passively ellipticals are significantly different to the models used to derive Eq. 1.

An error in one or both zero points can shift the entire C-M diagram either up or down. By using 2MASS stars in the field (see Sec. 2.2), we measured a mean colour difference of 0.009 magnitudes between the colour corrected HAWK-I colours and the 2MASS colours. We do not correct for this offset.

Another source of systematic error comes from the matching of the PSFs in the J and Ks-band images. An error in matching the PSFs will result in a offset in the colours, since the colours are computed from fixed apertures. We evaluate the likely size of this offset by comparing the colours of bright unsaturated stars in two different apertures: a 12 pixel diameter aperture and a larger $4''$ radius aperture. The average offset is 0.015 magnitudes with no evidence for a dependence on where the star was located in field-of-view. When this offset was larger than 0.02 magnitudes

³ <http://www.eso.org/instruments/hawki/>

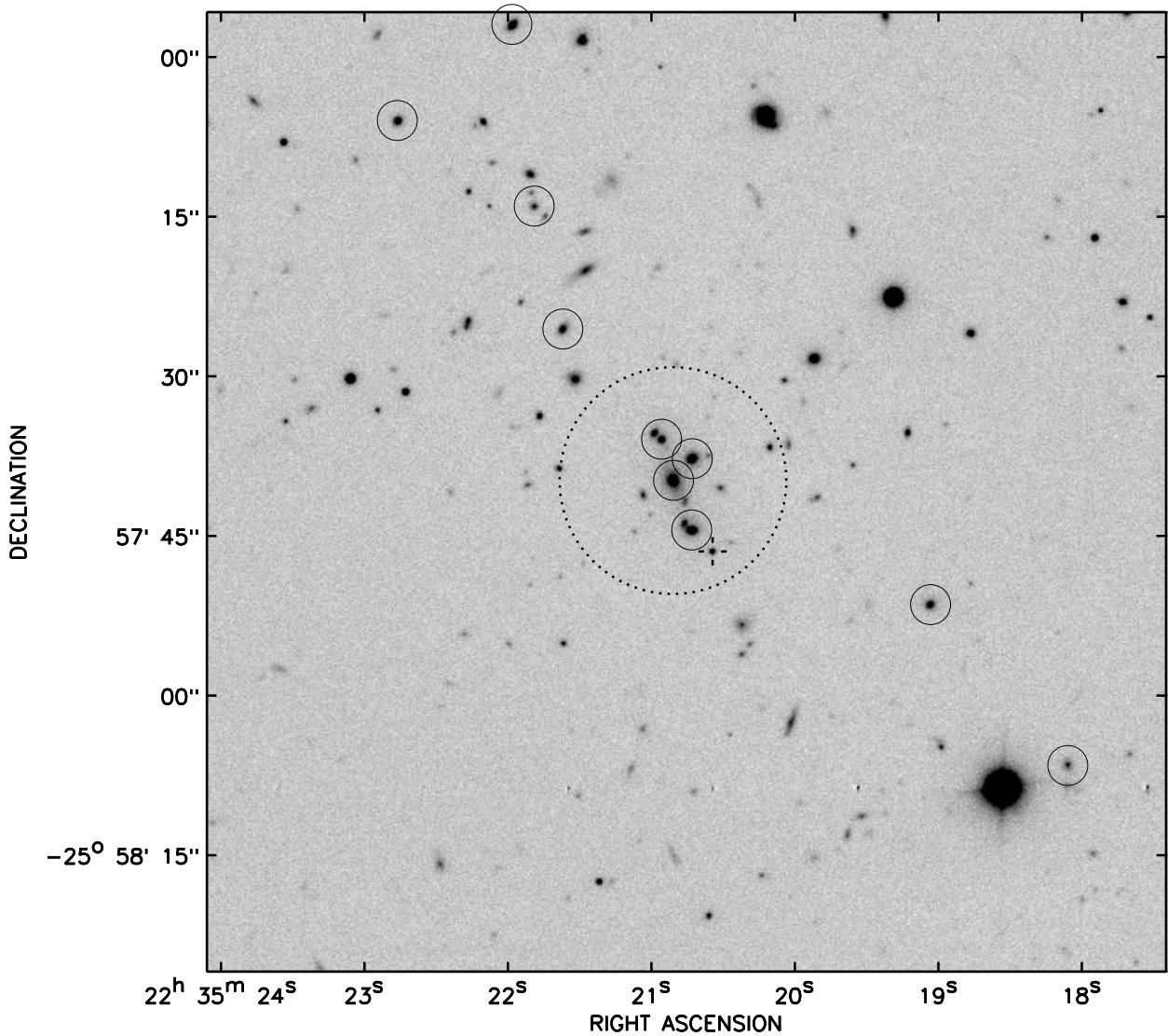


Fig. 1. HAWK-I Ks-band image of XMMU J2235.3-2557. Only the central 1% of the entire Ks-band image is shown here. The image is approximately $90''$ on a side, which, in the adopted cosmology, corresponds to 765 kpc at $z = 1.39$. Spectrally confirmed cluster members (Rosati et al. in preparation) are marked with circles. The star that is close to the cluster centre is also marked. The dotted circle that surrounds the central region of the cluster has a diameter of $21''$, which corresponds to 180 kpc at $z = 1.39$. The C-M relation (the solid red line in Fig. 2) is determined from galaxies that lie within this circle.

(just one case), we corrected the colours by this offset. Hence, a suitable value for this error is 0.02 magnitudes.

Although the resolution of these images are excellent for images that are taken from the ground, faint galaxies that lie near to the line of sight to brighter galaxies might go undetected. It is difficult to quantify the effect of these galaxies, but, qualitatively, since they are likely to be bluer, they will bias the colours of the red sequence galaxies to bluer colours.

3. The C-M diagram

The region surrounding the centre of XMMU J2235.3-2557 is shown in Fig. 1. The centre of the cluster and, in particular, the brightest cluster galaxy (BCG) are very conspicuous in the HAWK-I near-IR images. About half of the IR light in this central region comes from the BCG.

The colour magnitude diagram of selected targets in a region centred on the cluster is shown in Fig. 2. Galaxies within 100 pixels (90 kpc) of the centre of the cluster (within the dotted circle that is drawn in Fig.1) are plotted as large red circles.

Of these, four are spectroscopically confirmed cluster members⁴ and are replotted with open red squares. The [OII] $\lambda\lambda$ 3727 emission line is not detected in any these galaxies. Within this central region, there is one star, which is plotted as such in Fig. 2.

The continuous red line is a fit to the galaxies that lie within the central region and within the blue rectangle. The fit and the intrinsic scatter were determined by adjusting the intrinsic scatter until the reduced χ^2 of the fit was one. Since the errors in the photometry are small, the intrinsic scatter is very similar to the measured one and is 0.055 ± 0.018 magnitudes. A Monte-Carlo simulation was used to compute the error in our estimate of the intrinsic scatter. We ran 1000 realisations of the data with properties identical to the real one (magnitudes and photometric errors) and treated these realisations in the same way as the real data. The error was then estimated from the distribution of the fitted intrinsic scatter.

Our estimate of the intrinsic scatter is not very sensitive to the exact size of the region that is used to include galaxies. Doubling or halving the size of the region changes the intrinsic scatter by less than 0.01 magnitudes. Nor is it very sensitive to the precision at which we have estimated photometric errors. Doubling the size of the photometric errors reduces the intrinsic scatter by 0.01 magnitudes.

Although not all of the galaxies within the blue rectangle are spectroscopically confirmed cluster members, it is likely that most of them are cluster members. Using galaxies within the 13.5×13.5 field of view that was imaged by HAWK-I, we estimate that one galaxy would, by chance, lie within 100 pixels of the cluster centre and within the limits specified by the blue rectangle.

Outside this central region, spectroscopically confirmed cluster members with and without [OII] emission (11 and 7 members, respectively) are plotted as the small blue squares and small red circles, respectively. Isolated objects (objects that SExtractor does not identify as a merged detection) within 0.03 degrees (0.9 Mpc) of the cluster centre and generally without spectroscopic redshifts are plotted as black dots. The size of this region was chosen as a balance between having enough points to illustrate the colour of objects outside the cluster and obscuring the plot with too many points. The objects that make up the slightly tilted sequence at $J - K_s \sim 0.8$ are most likely evolved late type stars in the Galaxy. If one were to increase the size of the region, a second, less well defined sequence appears at $J - K_s \sim 0.4$.

4. Discussion

Galaxies within 90 kpc of the centre of the XMMU J2235.3-2557 lie on a well defined red sequence. The slope (-0.045 ± 0.019) and the scatter (0.055 ± 0.018 magnitudes) are similar to those measured in the X-ray luminous galaxy cluster RDCS J1252.9-2927 at $z=1.24$ (Lidman et al. 2004; Demarco et al. 2007).

Outside this central region the red sequence is far less well defined. Although the number of spectroscopically confirmed cluster members is rather modest and one must bear in mind the selection bias that comes from the relative ease in measuring the redshifts of star forming galaxies, it is clear that the galaxies outside the cluster centre are considerably more active. The [OII] emission line is seen in more than half of these galaxies.

Cluster members with [OII] emission have a broad colour distribution, from $J - K_s \sim 1.2$ to $J - K_s \sim 2.3$. Some of the [OII] cluster members land on the red sequence, thus agreeing with the notion that the [OII] emission line is a more sensitive indicator of active star formation or AGN activity (Yan et al. 2006) than galaxy colour. The two reddest cluster members are [OII] emitters and both are significantly redder than the red sequence, perhaps indicating the presence of significant amounts of dust in these galaxies. Outside the cluster centre, the two brightest cluster members are also [OII] emitters.

On the other hand, cluster members that are outside the cluster centre and without detectable [OII] emission either land on the red sequence or slightly blue of it, perhaps indicating that some of these galaxies are significantly younger than galaxies in the central part of the cluster. Alternatively, these galaxies could be bluer because there was a burst of star formation that ended just before these galaxies were observed. Photometry in bluer pass-bands and/or deep spectroscopy of these galaxies can be used to distinguish between these two possibilities.

Mullis et al. (2005) noted that two galaxies (one in the cluster core and another in the cluster outskirts) might be located in the foreground of the cluster. Removing these galaxies from the sample, does not significantly change the results.

4.1. The location of the red sequence

The location of the red sequence was modelled with the Bruzual & Charlot (2003) population synthesis code. We adopted a simple stellar population (SSP) model with a Salpeter initial mass function, Padova 1994 evolutionary tracks and no dust extinction. We did not model more complex star formation histories because of the limited colour information available (for a more extended analysis, see Rosati et al. in preparation). In order to reproduce the slope of the red sequence, the red sequence in the Coma cluster (Bower et al. 1992) was fitted with SSP models of varying metallicities. The model red sequence was then passively evolved back in time to $z = 1.39$. Model red sequences were computed for 5 different formation redshifts ($z_f=5, 4, 3, 2.5$ and 2). They are plotted as the dashed green lines in Fig. 2. Note that the modelling is based on the assumption that the slope of the red sequence is entirely due to the mass-metallicity relation. The close match between the observed slope (the continuous red line in Fig.2) and computed ones (the dashed green lines in Fig.2) suggests that this is a reasonable assumption.

Galaxies within the central 180 kpc are clearly old. The models suggest that the average formation redshift of the stars in these galaxies is $z_f \sim 4$. As discussed in the previous section, there is a systematic uncertainty of a few hundredths of a magnitude in the colours, which could move the average formation redshift to as early as $z_f = 4.5$ or as late as $z_f = 3.5$. This redshift is similar to the estimated formation redshifts of distant clusters that are at slightly lower redshifts. In RDCS J1252.9-2927 at $z = 1.24$, for example, it is estimated that the average formation redshift is $z_f \sim 3.5 - 4$ (Blakeslee et al. 2003; Gobat et al. 2008).

Outside the central region, cluster members appear to be, on average, younger. More than half these galaxies show signs of active star formation and about half of those that do not are significantly bluer than galaxies on the red sequence. If we were to interpret the difference in colour as a difference in age, then these galaxies are about 1.5 Gyr younger.

One can compute the redshift at which the colours of these galaxies would become indistinguishable from the colours of galaxies on the red sequence if all the galaxies were allowed to evolve passively. Using the models that were used to fit the

⁴ In this paper, we define galaxies with redshifts that lie within the redshift interval $1.375 < z < 1.400$ as cluster members.

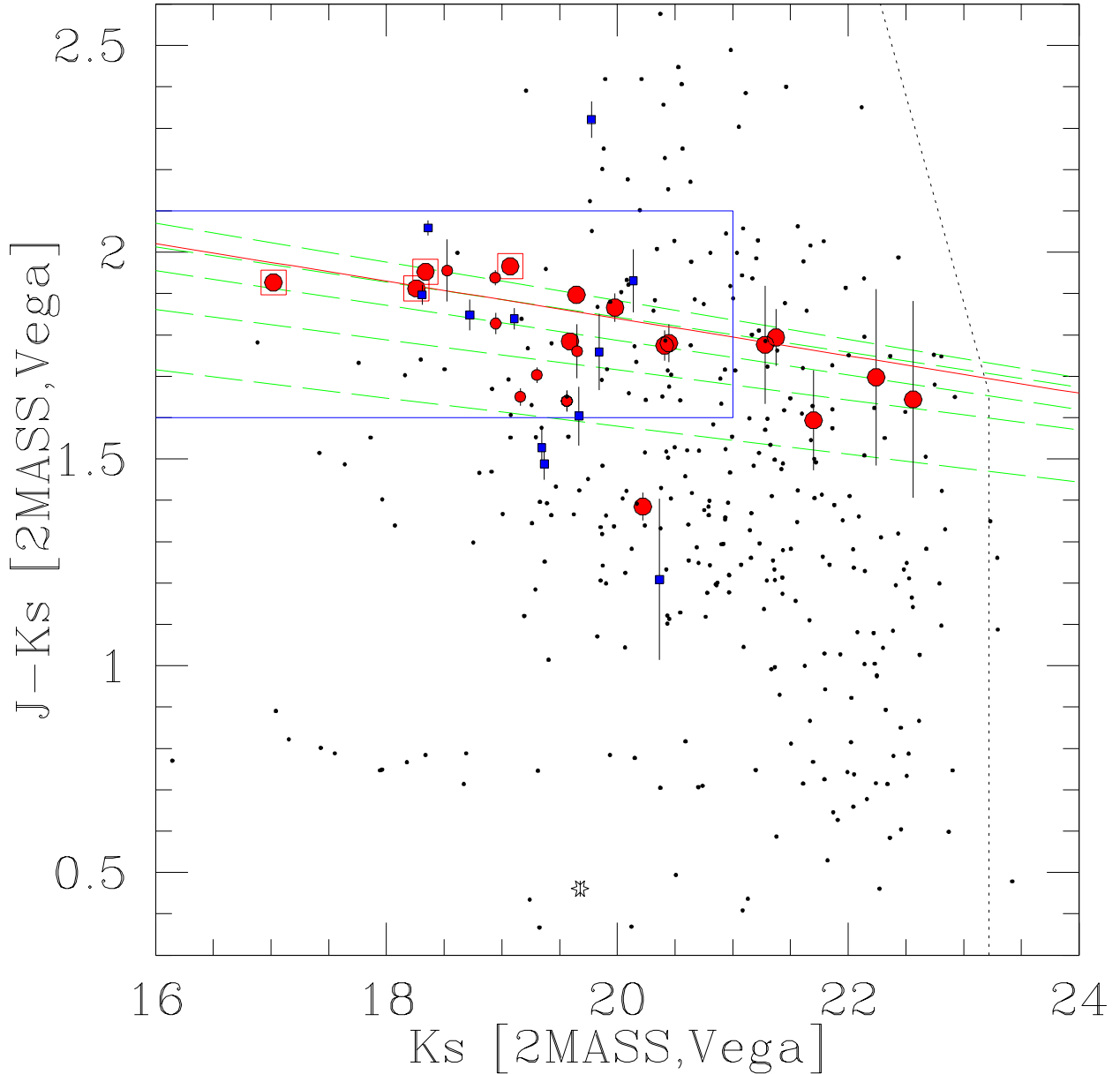


Fig. 2. Colour magnitude diagram of XMMU J2235.3-2557. Galaxies in the core of the cluster (within the dotted circle that is shown in Fig. 1) are plotted as large red circles. The continuous red line is a fit to the large red symbols that lie within the blue box. Four of these galaxies are spectroscopically confirmed cluster members and are replotted as open squares. The dotted lines represent the detection limits reported in Table 1. The near-horizontal dashed green lines are the result of evolving the red sequence of the Coma cluster backwards in time for different formation redshifts. From top to bottom, the formation redshifts are 5, 4, 3, 2.5 and 2. Cluster members that are outside the core are plotted as small red circles (for those that have no detectable [OII] emission) or small blue squares (for those that have [OII] emission). See the main text for details.

location of the red sequence, this occurs at $z \sim 1$, i.e., 1.3 Gyr later.

Alternatively, if the blue colours are caused by the presence of a young stellar population from a recently truncated episode of star formation, then these galaxies will join the red sequence more quickly.

The contrast between the cluster core, which is dominated by passively evolving galaxies on the red sequence, and the cluster outskirts, which is dominated by active galaxies spanning a wide range of colours, suggests that the red sequence of this cluster is

being built from the dense core of the cluster to relatively sparse outskirts. Furthermore, the process is a quick one. Many of the galaxies not currently on the red sequence will be on the red sequence by $z = 1$.

4.1.1. A flattening of the C-M relation at the bright end?

The colours of the four brightest galaxies in the centre of the cluster, which cover a range in brightness of a factor of five, are very similar, suggesting that the slope of the C-M relation is

flat at the bright end. A flattening in the C-M relation had also been noted in the X-ray luminous cluster RDCS J1252.9-2927 at $z=1.24$ (Demarco et al. 2007). If the flattening is real, then the C-M relation at fainter magnitudes becomes steeper.

At this stage, the flattening is only suggestive, since the number of bright galaxies over which it can be measured is small. Additional observations of other high redshift clusters will be required to confirm or refute the trend.

Dry red mergers - the merging of two passively evolving galaxies without subsequent star formation - is a process that can lead to a flattening of the C-M relation. For example, a 1:1 merger will result in a galaxy that is 0.75 magnitudes brighter and displaced by 0.035 magnitudes blue-wards of the C-M relation.

However, if dry red mergers were the cause for the flattening at the bright end, then one would expect this structure to persist as the cluster evolves, as all the galaxies at the bright end would have similar metallicities and ages. Although a flattening at the bright end of the C-M relation is evident in some semi-analytic N-body hierarchical galaxy formation models (De Lucia et al. 2004a; Menci et al. 2008), it has not been observed in well studied clusters at lower redshifts (e.g., Terlevich et al. 2001; Andreon 2006; Eisenhardt et al. 2007).

Alternatively, wet mergers - the merging of galaxies with subsequent star formation - may be responsible for part of the apparent flattening. In Fig. 2, the BCG is slightly bluer than expected. Since the [OII] line was not observed in the spectrum of the BCG, the slightly blue colours could be the result of recent but now extinguished burst of star formation that was triggered by a merger. Over time, the effect of this burst on the colour will fade and the colour of the BCG will move back towards the C-M relation.

4.1.2. Truncation of the red sequence

The continuous red line in Fig. 2 is a fit to the colour of galaxies in the core of the cluster. Although only galaxies within the blue box of Fig. 2 were used in the fit, there are galaxies outside this box that also lie close to this line.

Bearing in mind that some fainter galaxies might go undetected because of the crowded nature of the cluster centre, that not all of the galaxies plotted as large symbols in Fig. 2 have been confirmed as cluster members, and that the number of galaxies in this plot is quite small, there is no evidence that the red sequence is strongly truncated at $K_s \sim 20.5$, as was detected in the large scale structure surrounding RDCS J1252.9-2927 at $z=1.24$ (Tanaka et al. 2007) and in several proto-clusters (Kodama et al. 2007).

Hence, in this property, the core of XMMU J2235.3-2557 is similar to the core of RDCS J1252.9-2927. However, it remains to be tested if the luminosity function of galaxies within the large scale structure surrounding the core of XMMU J2235.3-2557 is truncated, as has been observed in RDCS J1252.9-2927.

4.2. The intrinsic scatter

While the tilt of the red sequence is largely due to a relationship between metallicity and luminosity and hence mass (brighter and larger galaxies are more metal rich) (Kodama 1999), the reason for the finite intrinsic scatter is less clear. It could be caused by variations in age, metallicity or a combination of both. Dust could also play a role. For early-type galaxies in the field, the scatter is caused by differences in age and metallicity

(Gallazzi et al. 2006), with variations in metallicity playing an increasingly important role as the mass of the galaxy increases.

The intrinsic scatter in the observer frame J – K_s colour of cluster galaxies about the C-M relation of XMMU J2235.3-2557 is 0.055 ± 0.018 magnitudes. Since only a few of the galaxies that were used to measure the scatter have been spectroscopically confirmed, it is possible, although unlikely, that the estimate of the scatter has been inflated by non-cluster members.

This scatter is similar to the scatter in observer frame J – K_s colours for galaxies in the X-ray luminous cluster RDCS J1252.9-2927 at $z=1.24$. (Lidman et al. 2004; Demarco et al. 2007). It is also similar to the scatter in the observer frame J – K colour measured for galaxies in clusters at lower redshifts (Stanford et al. 1998; Holden et al. 2004). Note, however, that the scatter reported here is in the observer frame, so the scatters are not directly comparable.

At $z = 1.39$, observer frame J and K_s approximately correspond to rest frame V and z. For Coma, the measured scatter in the V-I colour, the nearest colour for which the intrinsic scatter has been estimated, is 0.031 magnitudes (Eisenhardt et al. 2007). In detail, converting the intrinsic scatter from observer frame J – K_s to rest frame V – I or visa-versa requires an assumption of what causes the scatter (e.g., age, metallicity, or a combination of both) and a model of how this affects the spectral energy distribution. If the cause of the scatter is due to metallicity, for example, then, by using SSP models from Bruzual & Charlot (2003), the inferred scatter in rest frame V – I for galaxies in the core of XMMU J2235.3-2557 can be estimated and is found to be 0.035 ± 0.011 magnitudes, which is the same as that measured in Coma.

As seen in other studies (Stanford et al. 1998; Blakeslee et al. 2003, Mei et al. in preparation), the size of the scatter is remarkably constant. In this study, the scatter is constant over a time interval spanning 8.8 Gyr, which is a significant fraction of the age of the Universe. However, we should be aware of possible biases that are caused by the way low and high redshift samples are selected. In this particular case, the scatter measured for Coma was measured over a region that was several times larger than the region used for XMMU J2235.3-2557 (~ 1 Mpc versus ~ 0.2 Mpc). Even if similar size regions had been selected, it is likely that some galaxies that were outside the central region at $z = 1.39$ would by now lie within the central region and possibly visa-versa. This is a form of progenitor bias (van Dokkum et al. 2001), where the progenitors of youngest present day early type galaxies drop out of high redshift samples.

Of particular interest are cluster members that are significantly redder than the C-M relation. The most extreme example without [OII] in emission in XMMU J2235.3-2557 has a colour that is 0.08 magnitudes redder. The colour offset can easily be accounted for by an increase in the metallicity. In this particular example, an increase in the metallicity from $Z = 0.017$ to $Z = 0.023$ would account for the redder colour. On the other hand, if the redder colour was due to the galaxy being older and if errors have not been underestimated, then this galaxy would have to be as old as the Universe at $z = 1.39$.

4.3. Comparison with hierarchical galaxy formation models

The approach to modelling the behaviour of baryons in N-body hierarchical galaxy formation models comes in two main flavours: semi-analytical approaches (e.g. Kauffmann & Charlot 1998; De Lucia et al. 2004a; Menci et al. 2008), and hydrodynamical approaches (e.g. Romeo et al. 2008).

Here we make a qualitative comparison between the results from these models and the observations. A quantitative comparison requires detailed understanding of the quantities that are being measured in both the observations and the simulations. Such a comparison is beyond the scope of this paper.

In the hydrodynamical simulation run by Romeo et al. (2008), the fraction of galaxies actively forming stars strongly depends on environment and galaxy mass. For galaxies more massive than $2 \times 10^{10} M_{\odot}$, star formation first stops in the centre of the most massive clusters and then stops in the cluster outskirts or the centres of groups later.

In XMMU J2235.3-2557, which has an X-ray temperature that is slightly higher than C2 model of Romeo et al. (2008) (8-9 keV versus 6 keV), none of the galaxies in the core of the cluster are actively forming stars, whereas about half of the galaxies outside the core are. This picture is broadly consistent with the N-body simulations. However, we caution that the census of star forming galaxies in the centre and the outskirts of the cluster is far from complete.

There is, however, a notable difference between the models in Romeo et al. and the observations of XMMU J2235.3-2557. The slope of the red sequence in the models flattens with increasing cluster redshift and actually becomes positive. The flattening with redshift had also been noted in semi-analytical hierarchical simulations (Kauffmann & Charlot 1998; Menci et al. 2008). For galaxies in the core of XMMU J2235.3-2557, the slope of the red sequence is not positive, nor even flat. It is clearly negative.

As shown above, a simple model in which the galaxies form at very high redshift and evolve passively thereafter fits the slope of the C-M relation very well.

The semi-analytical and hydrodynamical simulations are also unable to reproduce both the size of the intrinsic scatter and the lack of evolution in the scatter with redshift.

In early semi-analytical simulations (Kauffmann & Charlot 1998), the scatter decreases with increasing redshift because the selection of galaxies in high redshift clusters is biased towards galaxies that have already formed at very high redshifts. From redshift zero to redshift 1.5, the scatter in the rest frame U-V decreases by a factor of ~ 2 (Kauffmann & Charlot 1998). In hydrodynamical simulations (Romeo et al. 2008), a similar decrease in the scatter is found for galaxies that lie on the dead sequence – galaxies that are no longer forming stars.

In more recent semi-analytic simulations (Menci et al. 2008), the average scatter up to $z = 1.5$ is almost independent of redshift, but is a factor of two to three larger than the observed value. Part of the discrepancy might come from the way red sequence galaxies are selected (Menci et al. 2008). In XMMU J2235.3-2557, however, all but one of the galaxies within the core of the cluster were used to compute the scatter, so the scatter in the core of this cluster is clearly small and consistent with Coma.

The scatter in the models of Menci et al. (2008) have a large range and the observations tend to land at the lower boundary of that range. This may indicate that the simulations consider a broader range of clusters and that the observations are biased to the most evolved examples. Alternatively, it might mean that the models are missing physical processes that lead to the small scatter.

5. Summary and Conclusions

We have presented near-IR observations of the X-ray luminous cluster XMMU J2235.3-2557 at $z = 1.39$ and we have built a

C-M diagram of objects inside and outside of the core of the cluster. While galaxies inside the cluster core form a well defined red sequence with no evidence of ongoing star formation, cluster members outside the core are much more diverse.

The colour of galaxies inside the core can be matched with SSP models that are ~ 3 Gyr old, corresponding to a redshift of formation of $z_f \sim 4$. These galaxies are already very old, especially when we consider that the cluster was observed at a time when the age of Universe was 4.6 Gyr.

Cluster members outside the core do not form a well defined red sequence. Over half these galaxies are forming stars and some of these are either considerably redder than the red sequence, perhaps indicating the presence of dust, or considerably bluer. The other half do not appear to be forming stars, but are, on average, displaced towards bluer colours, perhaps indicating that they either stopped forming stars recently or are younger than galaxies on the red sequence.

The contrast between the cluster core, which consists of a population of evolved galaxies with uniform colours, and the cluster outskirts, which consists of a population of active galaxies with diverse colours, suggests that the red sequence of this cluster is being built from the inside to the outside or, alternatively, from the dense core to the relatively sparse outskirts.

Acknowledgements. We acknowledge the very useful correspondence that we had with Andreas Seifahrt concerning the processing of HAWK-I data. This publication makes use of data products from the Two Micron All Sky Survey, which is a joint project of the University of Massachusetts and the Infrared Processing and Analysis Center/California Institute of Technology, funded by the National Aeronautics and Space Administration and the National Science Foundation. This research was supported by the Deutsche Forschungsgemeinschaft cluster of excellence program Origin and Structure of the Universe (www.universe-cluster.de).

References

- Andreon, S. 2006, MNRAS, 369, 969
 Andreon, S. 2008, MNRAS, 386, 1045
 Bell, E. F., Naab, T., McIntosh, D. H., et al. 2006, ApJ, 640, 241
 Bertin, E. & Arnouts, S. 1996, A&AS, 117, 393
 Blakeslee, J. P., Franx, M., Postman, M., et al. 2003, ApJ, 596, L143
 Bower, R. G., Lucey, J. R., & Ellis, R. S. 1992, MNRAS, 254, 601
 Bruzual, G. & Charlot, S. 2003, MNRAS, 344, 1000
 Casali, M., Pirard, J.-F., Kissler-Patig, M., et al. 2006, 6269
 Cohen, M., Wheaton, W. A., & Megeath, S. T. 2003, AJ, 126, 1090
 De Lucia, G., Kauffmann, G., & White, S. D. M. 2004a, MNRAS, 349, 1101
 De Lucia, G., Poggianti, B. M., Aragón-Salamanca, A., et al. 2004b, ApJ, 610, L77
 De Lucia, G., Poggianti, B. M., Aragón-Salamanca, A., et al. 2007, MNRAS, 374, 809
 de Vaucouleurs, G. 1961, ApJS, 5, 233
 Demarco, R., Rosati, P., Lidman, C., et al. 2007, ApJ, 663, 164
 Eisenhardt, P. R., De Propris, R., Gonzalez, A. H., et al. 2007, ApJS, 169, 225
 Faber, S. M., Willmer, C. N. A., Wolf, C., et al. 2007, ApJ, 665, 265
 Gallazzi, A., Charlot, S., Brinchmann, J., & White, S. D. M. 2006, MNRAS, 370, 1106
 Gilbank, D. G., Yee, H. K. C., Ellingson, E., et al. 2008, ApJ, 673, 742
 Gobat, R., Rosati, P., Strazzullo, V., et al. 2008, ArXiv e-prints, 806
 Hawarden, T. G., Leggett, S. K., Letawsky, M. B., Ballantyne, D. R., & Casali, M. M. 2001, MNRAS, 325, 563
 Holden, B. P., Stanford, S. A., Eisenhardt, P., & Dickinson, M. 2004, AJ, 127, 2484
 Homeier, N. L., Mei, S., Blakeslee, J. P., et al. 2006, ApJ, 647, 256
 Kauffmann, G. & Charlot, S. 1998, MNRAS, 294, 705
 Kodama, T. 1999, 163, 250
 Kodama, T., Tanaka, I., Kajisawa, M., et al. 2007, MNRAS, 377, 1717
 Labbé, I., Franx, M., Rudnick, G., et al. 2003, AJ, 125, 1107
 Lidman, C., Rosati, P., Demarco, R., et al. 2004, A&A, 416, 829
 Mei, S., Blakeslee, J. P., Stanford, S. A., et al. 2006, ApJ, 639, 81
 Menci, N., Rosati, P., Gobat, R., et al. 2008, ArXiv e-prints, 806
 Mullis, C. R., Rosati, P., Lamer, G., et al. 2005, ApJ, 623, L85
 Peng, C. Y., Ho, L. C., Impey, C. D., & Rix, H.-W. 2002, AJ, 124, 266

- Persson, S. E., Murphy, D. C., Krzeminski, W., Roth, M., & Rieke, M. J. 1998, *AJ*, 116, 2475
- Pirard, J.-F., Kissler-Patig, M., Moorwood, A., et al. 2004, 5492, 1763
- Romeo, A. D., Napolitano, N. R., Covone, G., et al. 2008, *ArXiv e-prints*, 804
- Schlegel, D. J., Finkbeiner, D. P., & Davis, M. 1998, *ApJ*, 500, 525
- Skrutskie, M. F., Cutri, R. M., Stiening, R., et al. 2006, *AJ*, 131, 1163
- Stanford, S. A., Eisenhardt, P. R., & Dickinson, M. 1998, *ApJ*, 492, 461
- Stanford, S. A., Romer, A. K., Sabirli, K., et al. 2006, *ApJ*, 646, L13
- Tanaka, M., Kodama, T., Arimoto, N., et al. 2005, *MNRAS*, 362, 268
- Tanaka, M., Kodama, T., Kajisawa, M., et al. 2007, *MNRAS*, 377, 1206
- Terlevich, A. I., Caldwell, N., & Bower, R. G. 2001, *MNRAS*, 326, 1547
- van Dokkum, P. G., Stanford, S. A., Holden, B. P., et al. 2001, *ApJ*, 552, L101
- Visvanathan, N. & Sandage, A. 1977, *ApJ*, 216, 214
- Yan, R., Newman, J. A., Faber, S. M., et al. 2006, *ApJ*, 648, 281
- Zirm, A. W., Stanford, S. A., Postman, M., et al. 2008, *ArXiv e-prints*, 802